

Self-Assembly of Octapod-Shaped Colloidal Nanocrystals into a Hexagonal Ballerina Network Embedded in a Thin Polymer Film

Milena P. Arciniegas,[†] Mee R. Kim,^{†,‡} Joost De Graaf,[‡] Rosaria Brescia,[†] Sergio Marras,[†] Karol Miszta,[†] Marjolein Dijkstra,[§] René van Roij,^{||} and Liberato Manna^{†,*}

[†]Istituto Italiano di Tecnologia (IIT), via Morego 30, IT-16163 Genova, Italy

[‡]Institute for Computational Physics (ICP), University of Stuttgart, Allmandring 3, 70569 Stuttgart, Germany

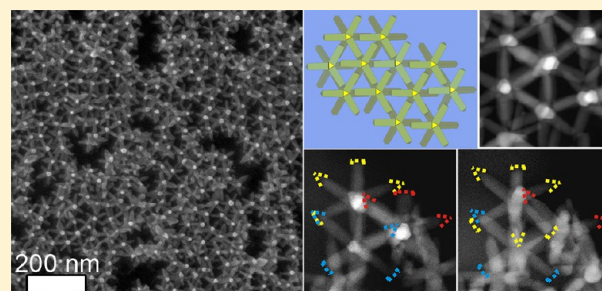
[§]Soft Condensed Matter, Debye Institute for Nanomaterials Science, Utrecht University, Princetonplein 5, 3584 CC Utrecht, The Netherlands

^{||}Institute for Theoretical Physics, Utrecht University, Princetonplein 5, 3584 CE Utrecht, The Netherlands

S Supporting Information

ABSTRACT: Nanoparticles with unconventional shapes may exhibit different types of assembly architectures that depend critically on the environmental conditions under which they are formed. Here, we demonstrate how the presence of polymer (polymethyl methacrylate, PMMA) molecules in a solution, in which CdSe(core)/CdS(pods) octapods are initially dispersed, affects the octapod-polymer organization upon solvent evaporation. We show that a fast drop-drying process can induce a remarkable two-dimensional (2D) self-assembly of octapods at the polymer/air interface. In the resulting structure, each octapod is oriented like a “ballerina”, that is, only one pod sticks out of the polymer film and is perpendicular to the polymer–air interface, while the opposite pod (with respect to the octapod’s center) is fully immersed in the film and points toward the substrate, like a ballerina performing a grand battement. In some areas, a hexagonal-like pattern is formed by the ballerinas in which the six nonvertical pods, which are all embedded in the film, maintain a pod–pod parallel configuration with respect to neighboring particles. We hypothesize that the mechanism responsible for such a self-assembly is based on a fast adsorption of the octapods from bulk solution to the droplet/air interface during the early stages of solvent evaporation. At this interface, the octapods maintain enough rotational freedom to organize mutually in a pod–pod parallel configuration between neighboring octapods. As the solvent evaporates, the octapods form a ballerina-rich octapod-polymer composite in which the octapods are in close contact with the substrate. Finally, we found that the resulting octapod-polymer composite is less hydrophilic than the polymer-only film.

KEYWORDS: Octapods, self-assembly, interface adsorption, polymer, nanocomposite



Colloidal branched nanocrystals (bNCs) have attracted scientific attention in recent years due to their potential use as building blocks of complex and functional superstructures with possible applications in the fields of nano-optoelectronics, photonics, or plasmonics.^{1–7} In contrast to isotropic nanocrystals, the self-organization of bNCs (especially those with long “branches”) into ordered superstructures can be hindered by intricate couplings between the translational and rotational degrees of freedom at high volume fractions of nanocrystals (the typical conditions under which ordered assemblies of colloidal particles are formed) and can cause them to get kinetically trapped into disordered, amorphous structures. Also, the mutual interactions between nanocrystals with complex shapes can be dominated by anisotropic van der Waals (vdW) forces, the strength of which is influenced by various factors including the shape of the bNCs, the type of stabilizing molecules bound at their surface, the solvent, and the NC concentration.^{8–11} This high dimensionality of the

parameter space can be used to potentially realize many different assembly symmetries, depending on the experimental conditions under which assembly is attempted, yet at the same time it complicates explicit predictions. Nevertheless, for branched octapod-shaped nanocrystals (referred to as “octapods” in the remainder of this paper) we recently demonstrated a fine control over shape and size,^{12,13} to the point that ordered superstructures of these nanocrystals have not only been experimentally observed but also theoretically explained by our groups.^{14–16} In fact, we have shown that different configurations of self-assembled octapods can be achieved both in bulk solution and on flat substrates; see Schemes I and II in Figure 1, respectively.^{14–16}

Received: December 20, 2013

Revised: January 15, 2014

Published: January 21, 2014

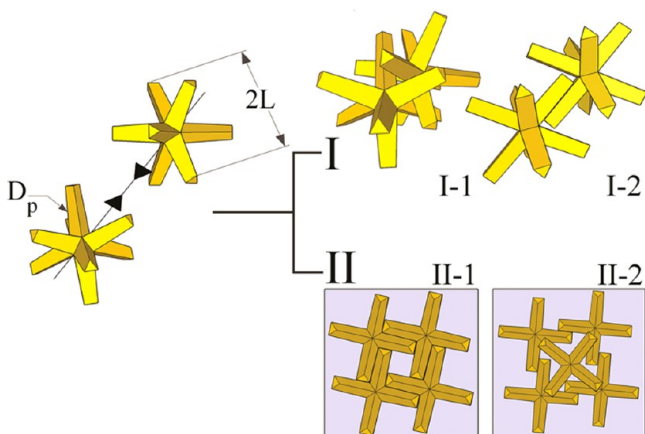


Figure 1. (Left) Sketch of two approaching octapods. For each octapod, the tip-to-tip length is $2L$, and the pod diameter is D_p . (Right) I. The two lowest energy configurations of an octapod–octapod dimer in bulk solution, as determined from theoretical calculations of the vdW interactions: (I-1) “interlocked” configuration and (I-2) pod–pod parallel configuration. Both configurations are involved in the experimentally observed formation of 3D octapod superstructures in solution.¹⁴ II. The experimentally observed (and calculated) 2D configurations of octapods on a flat substrate after solvent evaporation:¹⁶ Square-lattice (II-1) and binary square lattice (II-2).

In bulk solution, we experimentally demonstrated the formation of short linear chains of interlocked octapods (Scheme I-1 in Figure 1) through an aging process of an octapod-rich toluene solution. After the addition of acetonitrile longer linear chains were formed,¹⁴ followed by the self-assembly of the chains into a porous three-dimensional (3D) superstructure with parallel pod–pod alignment (Scheme I-2 in Figure 1). Using theoretical calculations of the vdW interactions, we demonstrated that the interlocked and pod–pod parallel arrangements are energetically the most favorable configurations in bulk solution,¹⁴ thus explaining the experimental observations.

On flat substrates, we demonstrated instead that ordered monolayers of octapods can be formed in a side-to-side configuration through solvent evaporation. The monolayers could consist either of simple or binary square lattices, depending on the aspect ratio L/D_p of the pods (see Scheme II-1 and II-2 in Figure 1).^{15,16} In those experiments, both a fast solvent evaporation and the presence of the substrate limit the 3D rotation of the octapods and constrain the octapods to stand on four pods on the substrate, thereby preventing the formation of interlocked structures in the “coffee stain”. To date, octapod superstructures have thus been obtained by exploiting either the more favorable interlocked configuration in solution, or the additional constraint imposed by the presence of a flat substrate.

Apparently, assemblies with the pod–pod parallel configuration (Scheme I-2 in Figure 1) are difficult to realize, most likely because they require a good balance between steric repulsion at short distances and vdW forces to cause the two octapods to approach each other along parallel axes.¹⁴ This is far less likely to be achieved for single octapods in bulk solution, given their geometrical restrictions in addition to the steric/vdW balance requirement.¹⁷ In order to achieve the parallel pod–pod configuration for octapods, long pods are preferred over short ones. The reason is that the increased

contact area between longer pods in the pod–pod configuration causes stronger pod–pod vdW attractions, which can dominate over the core–core vdW attractions that stabilize the interlocked configuration. It should be noted that small-scale assemblies of tetrapodal branched NCs with parallel pod–pod configurations have already been reported. This type of organization was achieved both via the Langmuir–Blodgett technique and by exploiting attractive depletion forces in a surfactant-rich (or polymer-rich) solution of NCs.^{18,19}

In this work, we demonstrate the formation of superstructures of octapods that fully exploit the parallel pod–pod configuration. Such an assembly was serendipitously discovered upon drying a solution of octapods and excess unwashed organics on a SiO_2 substrate at room temperature in a solvent-saturated atmosphere. Here, the excess organics, which stem from the synthesis, are impurities mainly consisting of free unbound surfactants and Cd-phosphate complexes. Scanning electron microscopy (SEM) analysis of the sample after evaporation evidenced a ringlike deposit on the substrate with a primarily hexagonal-like structure as discerned from the top view shown in Figure 2a.

Figure 2a, which was acquired with a low-angle backscattered electron detector (LBE), reveals that the edges of the hexagons are formed by six pairs of pods from neighboring octapods (some of the hexagons are framed in yellow in Figure 2a to illustrate this). For each octapod belonging to this superstructure, only one tip was observed when the same zone was scanned with an upper secondary electron detector (SEI), see Figure 2b. This image shows a strong contrast between the octapods (bright posts) and the organic film (light gray); see also a top view of the structure in the Supporting Information Figure S1a,b. A SEM image of the same zone, using a lower secondary electron detector (LEI), Figure 2c, demonstrates that the octapods are standing upright with one pod on the substrate (see the inset), in what we refer to as a “ballerina” configuration forming the hexagonal network (see sketches in Figure 2d).

Starting from this point, we intentionally prepared mixtures of octapods with a conventional polymer (polymethyl methacrylate, PMMA) in order to improve the control over the self-assembly process into this “ballet of nanoballerinas”. For this purpose, we first washed the octapods several times to remove the excess of organics that derived from the synthesis. This cleaning was also useful to improve the dispersion of octapods in the polymer solutions and to ensure a more direct contact with the polymer. As screening experiments, we mixed solutions of PMMA and octapods in toluene at different concentrations to estimate the solubility threshold using (i) the turbidity of the solution as a first sign of aggregation, and (ii) dynamic light scattering measurements to assess the size of aggregates after the addition of the polymer. We also varied the molecular weight of the polymer, M_w , in these experiments, see Supporting Information Figure S2. We found that polymer concentrations above 5% vol induced visible aggregation of octapods in PMMA solutions, especially for high M_w . Therefore, the concentration of PMMA (with $M_w = 120\,000$ g/mol) was maintained far below 5% vol in the subsequent experiments. This ensures a large number of well-dispersed octapods in the toluene-PMMA solution, right before the toluene evaporation and the film formation. Also the concentration of octapods in the composite solution was found to play an important role, since large-scale self-assembly requires a sufficiently high initial concentration. For an octapod

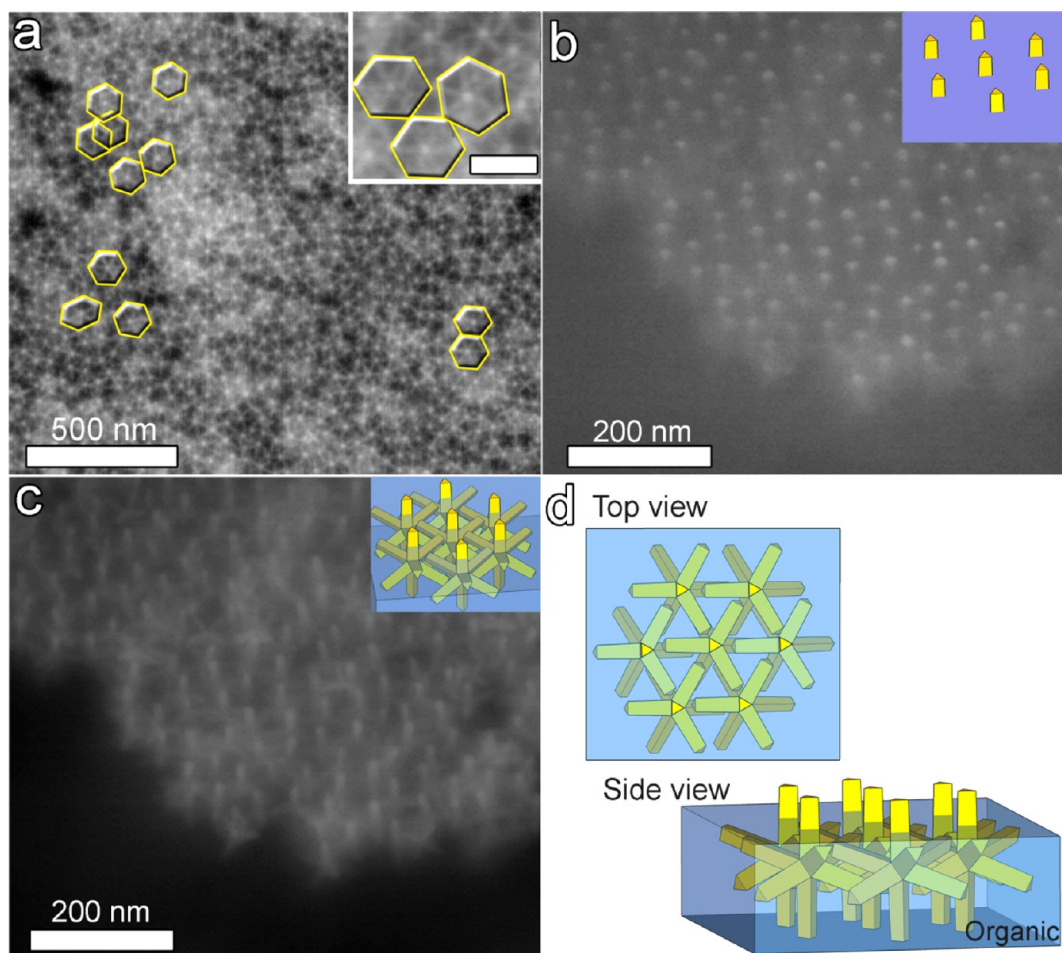


Figure 2. Arrangement of octapods after slow drying of a drop from an organic-rich toluene solution. (a) LBE-SEM top-view image revealing the self-assembly of octapods into a hexagonal-like structure in the coffee-stain region formed on the SiO₂ substrate; the inset shows a close-up view of the same image. (b) A 45°-tilt-SEI-SEM image demonstrating the presence of the organic residues (light gray); for each octapod only the upper section of the pod pointing upward actually protrudes out of the organic film (see sketch in the inset). (c) A 45°-tilt-LEI-SEM image of the same zone evidencing that the remaining seven pods are inside the organic layer (see sketch in the inset). (d) Sketches summarizing the observed assembly in both top and side view.

concentration below 10^{-7} M only small-scale structures were formed independent of the PMMA concentration (see Supporting Information Figure S3a).

In another series of experiments, drops from repeatedly washed octapod solutions with no added polymer, as well as drops from octapod-polymer mixtures, were cast on carbon-coated Cu grids for transmission electron microscopy (TEM) and on a 10 nm carbon-coated SiO₂ wafer. Both types of substrate have poor hydrophilic character, which should help to avoid ringlike deposits. The solvent was allowed to evaporate in air (yielding a faster evaporation rate) at room temperature (25 °C) and relative humidity of 55%. When polymer-free octapod solutions were drop-cast, we found after sufficiently fast evaporation that the octapods had four pods in contact with the substrate (see Figure 3a and Supporting Information Figure S1d). These octapods formed short-ranged 2D-ordered structures in some areas, depicted by the sketch in Figure 3a, similar to the square-lattice configuration reported by us in a previous work.¹⁶ However, for sufficiently slow evaporation we found for the same polymer-free octapod solution mainly interlocked chain-like assemblies, similar to those reported in another one of our papers¹⁴ (see Supporting Information

Figure S1c). This exemplifies the key role of the excess organic residues in the self-assembly of the ballerina configuration.

A remarkably different self-assembled network of octapods was obtained after adding PMMA at 1% vol to the NC solution (1:4 volume ratio of octapod/PMMA solution). Drop-casting the octapod-polymer mixture and evaporating the solvent (see Figure 3b) yielded a network of octapods with a primarily hexagonal-like structure, as evidenced in the inset in Figure 3b. Also, the octapods in this configuration were partially immersed in the PMMA layer (which appears as the intermediate gray level in Figure 3c). The thickness of the PMMA layer embedding the ballerina assemblies on the C-support film on the TEM grid was estimated to be 71 ± 7 nm by evaluating the inelastic scattering undergone by electrons in the TEM (log-ratio method, see Supporting Information);²⁰ this thickness is about 73% of the tip-to-tip distance $2L$ of an octapod (see the left sketch of Figure 1). A tilted SEM image of the structure demonstrated that the octapods have one pod sticking out of the polymer/air interface (bright posts in Figure 3d), forming the ballerina configuration in the PMMA.

Detailed SEM observation of samples from which the polymer was removed by an oxygen plasma treatment confirmed that the ballerina-hexagonal arrangement of the

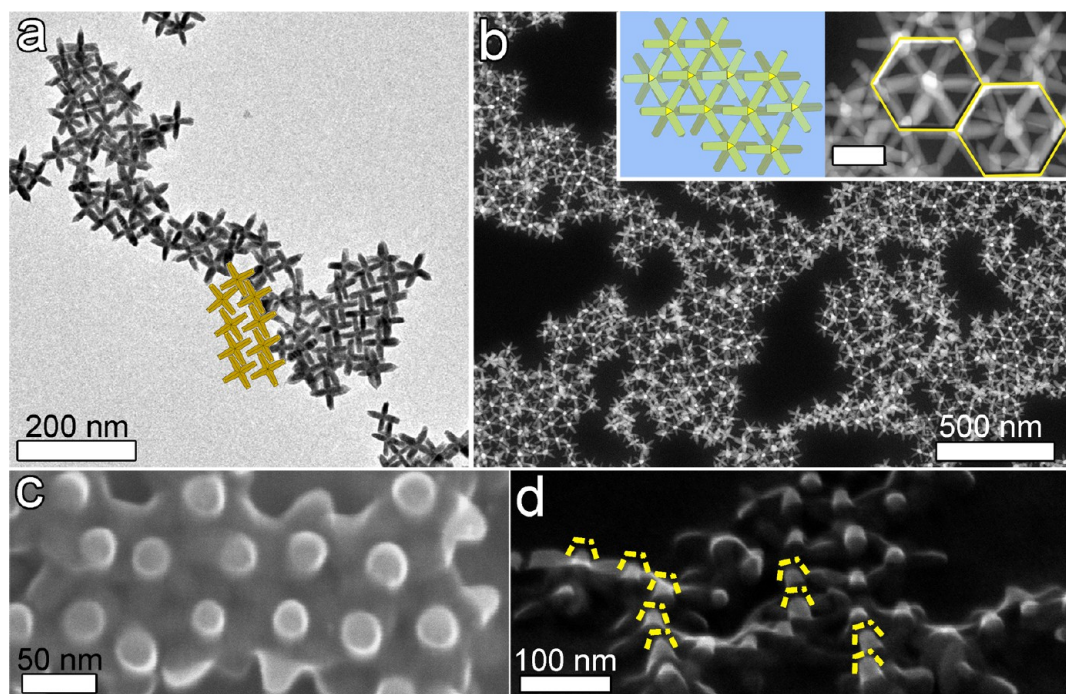


Figure 3. (a) TEM image of the repeatedly washed toluene suspension with octapods after fast solvent evaporation. The particles are touching the substrate (carbon support film on Cu grid for TEM) with four pods. Most of the octapods formed a short-ranged square-lattice-like structure. The cartoon embedded in the figure highlights the octapod pattern. (b) HAADF-STEM image showing the self-assembled ballerina network of octapods formed after drop-casting of PMMA-octapod solutions (PMMA at 1% vol) and fast solvent evaporation; the insets evidence the locally regular hexagonal-like structure. Scale bar: 50 nm. (c) Top-view SEM image of the sample in (b) that confirms the ballerina configuration, also showing that the octapods are partially embedded in the polymer. (d) A 45°-tilt-SEM image in which the single protruding pod from each of the embedded octapods can be discerned (framed in yellow dashed lines).

octapods consisted of one single layer on the substrate (see Figure 4a). This arrangement was further confirmed by HAADF-STEM images taken at different tilt angles (see Figure 4b, Supporting Information Figure S4 and movie S11.avi and S12.avi). The pod-pod parallel configuration of neighboring octapods is indeed consistent with the hexagonal-like arrangements of the bright posts viewed in SEM (Figure 2) and in HAADF-STEM plan-view images (Figure 3b).

This superstructure formation is reminiscent of the self-assembly of NCs induced by liquid/air interface techniques, which result in uniform distributions of NCs at the interface under equilibrium conditions.^{18,21–24} Unlike controlled solvent evaporation, which given enough time is in favor of 3D ordered structures, fast solvent evaporation forces the nanoparticles out of equilibrium and may drive the system toward a different self-assembled state.^{25–27} The formation of the ballerina network must be a consequence of the addition of the PMMA to the octapod solution, because in the absence of the PMMA no ordered domains with the ballerina configuration were observed. Moreover, we note that the observed hexagonal-like arrangements of ballerina octapods are not densely packed, which indicates that the forces exerted during drying are insufficient to drive the octapods to their optimal packing, in contrast with the results obtained for drop-cast, slow-dried solutions of octapods without PMMA added.^{15,16} This suggests that forces other than those caused by drying play a dominant role during the later stages of the self-assembly. Hence we hypothesize that the octapods reach the observed ballerina configuration in the following three stages:

- Stage I (Figure 4c-I): immediately after drop deposition, the octapods are free to diffuse through the toluene-PMMA

medium, as the viscosity of the solution is still low. The fast evaporation of the toluene, however, tends to force the octapods to the droplet-air interface. This process can be explained by considering the octapod diffusion coefficient D in the solution. The octapod diffusion is time-dependent due to the changes in the viscosity η of the medium during drying, as can be seen from the Stokes-Einstein equation for nanoparticles with a hydrodynamic radius r , given by $D = k_B T / 6\pi\eta r$ with k_B as the Boltzmann constant and T as the temperature. Because of the increase in the viscosity of the PMMA-solution during the toluene evaporation, the diffusion of the octapods D decreases significantly. This causes the octapod movement to eventually become slower than the advancement rate of the polymer-air interface, thereby forcing the octapods to the interface.

- Stage II (Figure 4c-II): at the interface, the free energy of adsorption causes the octapods to adopt a specific, albeit yet unknown, orientation. It should be noted that the vertical constraint provided by the interfacial energy that forces the octapods to remain trapped at the interface does not hinder its lateral movements. In this stage, as reported in other works on interfacial self-assembly,^{28–32} the adsorption of the octapods at the interface could induce the formation of a capillary multipole structure around the NCs. The multipolar octapod-octapod capillary interactions may then facilitate the octapods coming together in a specific way. For instance, the octapods could approach each other with their pods almost aligned, leading the way for interactions that dominate the multipolar component at short ranges to take over, causing the already prealigned octapods to self-assemble into a pod-pod ballerina network. However, it is equally possible that the droplet shrinking due to

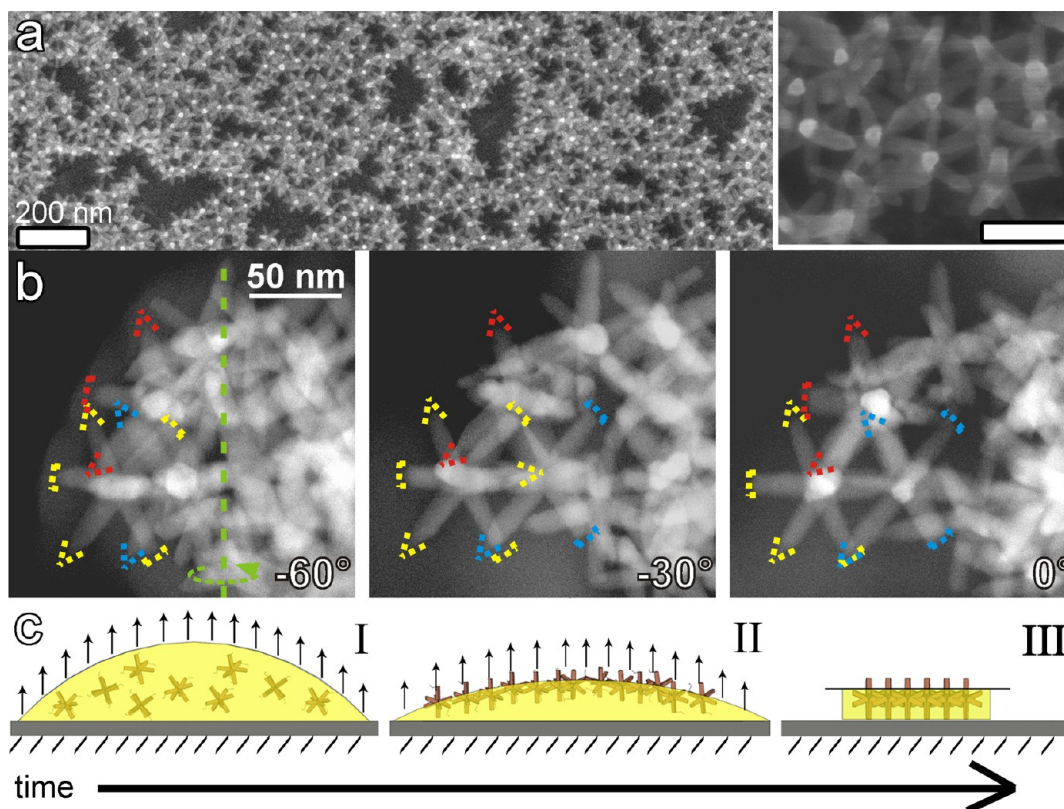


Figure 4. (a) SEI-SEM image after removing the polymer (via an oxygen plasma treatment) evidencing that the ballerinas are standing on the substrate. The inset shows a close-up view of an ordered domain. The scale bar is 60 nm. (b) HAADF-STEM images at different tilt angles confirming the pod–pod parallel arrangement between octapods forming the hexagonal array of ballerinas. (c) Cartoon explaining the formation of the ballerinas at the droplet/air interface. (I). The particles are constrained to move toward the interface and remain trapped there during drying; weak vdW and interfacial interactions are responsible for the pod–pod configuration (II–III).

fluid evaporation is the dominant term in the drying forces that cause the octapods to be driven together. Moreover, capillary attractions and interfacial deformation could only play a subdominant role in the formation of the ballerina network. In this scenario, the final step of the self-assembly might then be entirely caused by other effects, such as substrate-mediated orientational ordering. We therefore conjecture that in Stage II the octapods are driven together by a combination of droplet shrinking and capillary attraction, both of which may dominate the aggregation of the octapods at different points during the drying.

- Stage III (Figure 4c-III): when the octapods are in mutual close proximity, they start to interact presumably mostly through vdW forces, since the ballerina network shows pod–pod configurations. Drying and adsorption free energies are apparently sufficiently slow and low, respectively, to allow the octapods to reorient from their adsorbed orientation to one where they form pod–pod parallel arrangements with their neighbors (see the inset in Figure 4a and Figure 4b), rather than be forced together into a densely packed state. As mentioned in the description of Stage II, the reorientation may be induced by multipolar interactions stemming from the deformation of the interface, but could equally well be caused by a host of other forces, including restrictions imposed by the substrate.

In our description of the various stages, we stated that interfacial adsorption could play a significant role in the self-assembly mechanism, since it might favor a configuration that facilitates octapods forming pod–pod contacts through vdW

forces rather than interlocked or dense-packed configurations; the interfacial adsorption may even prevent the formation of interlocked contacts via a free-energy penalty. Therefore, we calculated the adsorption free energy for the octapod/polymer system (see Supporting Information for additional details) in order to gauge the relevance of adsorption on the formation of the ballerina configuration. Similar calculations have proven their usefulness in clarifying the adsorption of nanoparticles at fluid interfaces and the self-assembled structures that these particles formed.²¹ In our calculations, we considered the optimal adhesion at a flat nondeformable toluene–air interface for a single octapod as a function of the (cosine of the) contact angle ($\cos \theta$ in Figure 5) between the octapod material and the solvent interface,^{33,34} as the system's wettability depends on the solvent (with polymer)–octapod, air–octapod, and solvent–air

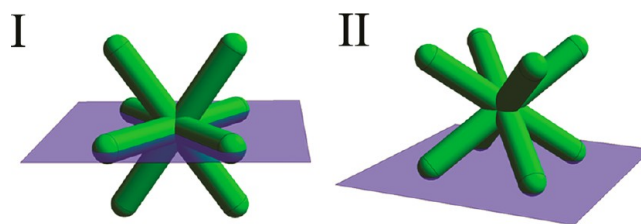


Figure 5. The archetypical configurations for an octapod adsorbed at a flat nondeformable interface between air (below) and toluene/polymer (above) for a cosine of the contact angle in the range (I) $0.0 \leq \cos \theta \leq 0.3$ and (II) $0.3 < \cos \theta \leq 0.9$; the octapod is fully detached for $\cos \theta > 0.9$.

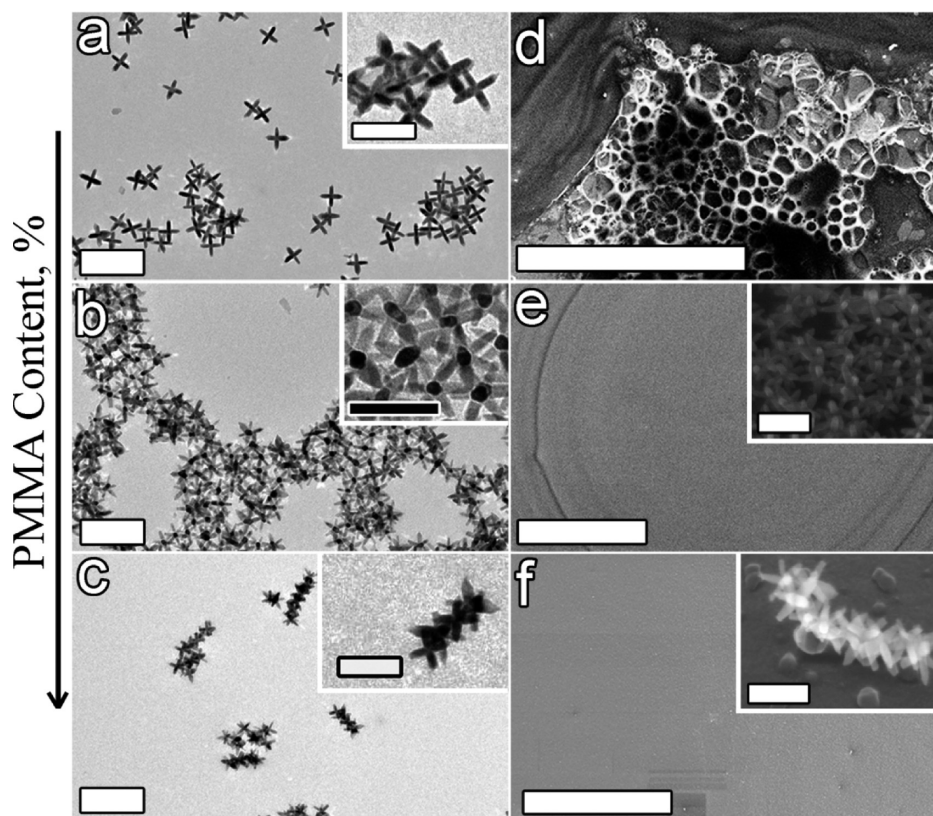


Figure 6. (a–c) TEM images of the PMMA-based nanocomposite revealing how octapod configurations depend on the polymer content/thickness. (a) Octapods standing on four-pods touching the substrate with an evident strong dewetting of the polymer (PMMA 0.5% vol.) on the substrate as can be seen in panel d; scale bar: 200 nm. (b) Octapods in the ballerina configuration (PMMA 1.0% vol.). (c) Interlocked octapods forming short chains (PMMA 5.0% vol.); the insets show a close-up view of each arrangement; scale bar: 50 nm. (d–f) SEM images evidence the morphology of the films depending on the polymer content; scale bars: 200 nm. Strong dewetting for more diluted solutions (d) and a more uniform and thicker film from concentrated PMMA solutions loaded with octapods (e,f). The insets show a 30°-tilt-SEM image of the ballerina configuration and the chainlike interlocked octapods after removal of the polymer by oxygen plasma treatment.

surface tensions. We also limited ourselves to a single contact angle all over the octapod surface, thereby ignoring possible chemical and structural heterogeneities to avoid further complications in the analysis. However, even such a simple model can give insights into the behavior of bNCs at an interface. Our results suggest that the octapod's orientation and trapping at the interface can be strongly influenced by the wettability of the particles. However, they also show that the cause of the experimental observations is not to be sought solely in an adsorption mechanism, as neither of the orientations of octapods obtained here corresponds to the ballerina configuration (see Supporting Information Figure S4). We found instead two optimal trapping configurations, as shown in Figure 5, for which the octapods are partially wetted by the polymer solution: (I) four-arms lie flat on the interface and two stick out on either side and (II) the octapod rests on the interface with four tips slightly penetrating it. We refer to these configurations as archetypical, because over the range of contact angles that we considered there are only slight variations in the exact position and orientation of the octapod at the interface with respect to these two configurations (see Supporting Information Figure S4). However, there is a very sharp transition from configuration I to configuration II, with no intermediate states.

Our result can be explained by the way the system minimizes its free energy. When there is little difference between the media ($\cos \theta$ is small) the octapod excludes the maximum

surface area from the interface, while when the difference between the media is large ($\cos \theta$ is large) the octapod minimizes its contact with the energetically unfavored medium. This is true in general, since the free energy of adsorption can be lowered by removing part of the interface, but strongly hydrophobic/hydrophilic colloids would still prefer to minimize their contact with the unfavored medium.²¹ Note that neither of the archetypical configurations corresponds to the observed ballerina configuration. We therefore conjecture that the ballerina configuration is unlikely to be explained by adsorption to the interface alone, since the ballerina configuration itself does not exclude a particularly big part of the interface, nor does it seem to minimize contact with the air. Moreover, adding a polymer, which changes the contact angle properties of the system, is unlikely to prevent the octapods from being driven toward their dense-packed configuration in an adsorption-only self-assembly scenario. It is, however, possible that when the octapods are in close proximity the deformation of the interface aids in the formation of the ballerina network. The final state is likely achieved by the interplay between various effects, such as, adsorption, vdW forces, restrictions imposed by the substrate, and the slowing of the dynamics in the final stage of the self-assembly brought on by the increased viscosity of the solution.

Because the polymer content is known to strongly influence the adsorption properties, we considered the assemblies that formed upon varying the polymer content. We found different

octapod configurations in the PMMA film when the amount of polymer injected into the octapod solution was increased from 0.5 to 5% vol. (see Figure 6a–c). Octapods with four pods in contact with the substrate were observed for a PMMA concentration between 0 and 0.5% vol. A sharp change in the self-assembly behavior was observed when the PMMA concentration was increased up to 5.0% vol since ballerinas formed at 1% vol as we have seen already, and interlocked chains of 5–8 octapods were found in these films at 5% vol. This remarkable variation in configurations by changing the PMMA content is attributed to an increase in the number of polymer molecules wrapping the octapod surface, which can further lead to the formation of well-ordered aggregates by stronger octapod–octapod interactions.^{35–37} These conditions, however, are not in favor of the ballerina configuration, as both the viscosity of the solution and the thickness of the final film are increased with an increasing PMMA content. In this case, because the diffusion coefficient D of the octapods is drastically decreased, the movement of the octapods is limited and they are forced to remain embedded in the polymer film until the end of the solvent evaporation.

Our observations by SEM of the samples prepared on carbon-coated SiO₂ substrates revealed a strong dewetting of the polymer film on the substrate in the case of a more diluted PMMA solution (see Figure 6d), whereas samples containing larger amounts of PMMA resulted in more homogeneous films (see Figure 6e,f) because of the lower fluidity of the polymer. We observed a higher shrinkage of the polymer in the center area in the sample containing 1% of PMMA (see Figure 6e), which we attributed to the solvent evaporation rate. Measurements of the thickness of these films conducted by a nanoprofilometer indicated a variation from the center area to the edges of the drop spreading from about 68 to 100 nm and from 230 to 300 nm for 1 and 5% of PMMA, respectively. Removal of the polymer revealed that the ballerina configuration was obtained in the 1% PMMA film (see inset in Figure 6e) in the area with a thickness of ~70 nm, while interlocked octapods were observed for 5% PMMA content (see inset in Figure 6f).

In order to further study the impact of the ballerina network on the surface properties of the PMMA composite film, we evaluated how this configuration affects the contact angle of water wetting the film. Contact angle measurements were performed using the sessile-drop method with ultrapure water (see the Supporting Information for details). Figure 7 shows the mean contact angle determined on the octapod-PMMA thin film deposited on carbon-coated SiO₂ substrates. Both a SiO₂ and a PMMA thin film on a carbon coated SiO₂ substrate were used as control materials.

The octapod/PMMA substrate gives rise to a significantly higher value of the contact angle than the references; after the formation of the ballerina network islands on the PMMA film, the contact angle increased significantly, that is, by more than 10° from 71.5 to 85.3°. This is attributed to the effect of the pod protruding from the polymer layer that is formed during the last stage of the evaporation in the thinner area of the film. Because of a variation in the polymer flow, the local roughness of the film may also be increased, thereby helping to pin the drop of water and inducing a more hydrophobic character in the hydrophilic PMMA.

In summary, we have presented a new assembly of octapod-shaped nanocrystals formed via fast drop casting of a PMMA/toluene/octapod solution on a flat substrate. The networks that

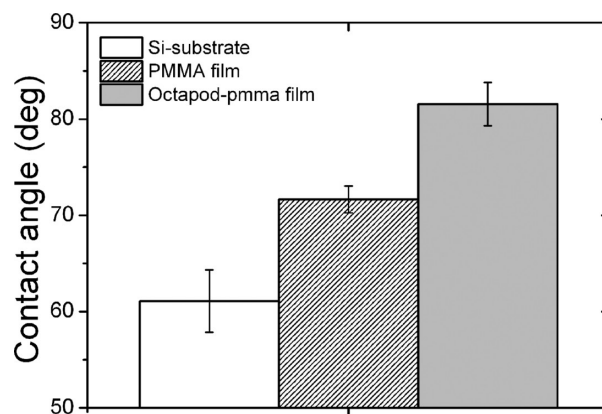


Figure 7. Contact angle with (ultrapure) water determined for the ballerina network on the PMMA film revealing loss of the hydrophilic character of the PMMA film attributed to the presence of the nanopinned surface formed by the octapods.

we observed consist of octapods partially immersed in a thin polymer film. These octapods stand on the substrate with one pod oriented perpendicular to the substrate, while the opposing pod slightly penetrates the polymer/air interface. Neighboring ballerina octapods have a parallel pod–pod arrangement between the remaining six pods that causes them to form a hexagonal-like lattice. We have studied how the octapod self-assembly changes with the increase in polymer content from the formation of nonordered aggregates at low polymer concentration to the formation of ordered hexagonal ballerinas or short linear chains at higher polymer concentrations. We relate this to an increased probability of attractive pod–pod interactions. We hypothesize that upon increasing the PMMA content, the adsorption of octapods at the interface, in combination with van der Waals interactions between the octapods, and the restrictions imposed by the substrate, are the key parameters that control the formation of the ballerina configuration. These ingredients might all play an important role during the different regimes of solvent evaporation of a viscous solution, where a droplet spreads and dries on a wettable substrate. We have demonstrated that the ballerina octapod-polymer composite has an enhanced hydrophobicity with respect to that of a pure polymer film. Better understanding of the key parameters involved in the formation of this unusual network will be the subject of follow-up studies, which may provide indications for the scaling-up of the process and the optimization of this structure, leading to its potential use in nanodevices. For instance, achieving a ballerina network in a polymer thin film may improve its structural and mechanical stability, as it might work as nanopinned network to impede crack propagation.

■ ASSOCIATED CONTENT

📄 Supporting Information

Additional information, figures, and videos. This material is available free of charge via the Internet at <http://pubs.acs.org>.

■ AUTHOR INFORMATION

Corresponding Author

*E-mail: liberato.manna@iit.it

Present Address

[†]Institut National de la Recherche Scientifique (INRS), Université du Québec, 1650 Boulevard Lionel-Boulet, Varennes, Québec, J3X 1S2 Canada.

Author Contributions

The manuscript was written through contributions of all authors. All authors have given approval to the final version of the manuscript.

Notes

The authors declare no competing financial interest.

ACKNOWLEDGMENTS

M.P.A., M.R.K., R.B., S.M., K.M., and L.M. acknowledge financial support from European Union through the FP7 starting ERC Grant NANO-ARCH (Contract Number 240111). J.D.G. acknowledges financial support from the NWO Rubicon Grant (680501210). Both R.v.R. and M.D. acknowledge financial support from an NWO-VICI grant. The authors would like to thank Dr. F. De Angelis, Dr. V. Lesnyak, and Dr. L. Ceseracciu for fruitful discussions.

REFERENCES

- (1) Li, H.; Kanaras, A. G.; Manna, L. *Acc. Chem. Res.* **2013**, *46*, 1387–1396.
- (2) Lim, B.; Xia, Y. *Angew. Chem., Int. Ed.* **2011**, *50*, 76–85.
- (3) Das, P.; Kedia, A.; Kumar, P. S.; Large, N.; Chini, T. K. *Nanotechnology* **2013**, *24*, 405704.
- (4) DeSantis, C. J.; Skrabalak, S. E. *Langmuir* **2012**, *28*, 9055–9062.
- (5) Fu, X.-L.; Peng, Z.-J.; Li, D.; Zhang, L.; Xiao, J.-H.; Li, J.-Y.; Fang, Z.-Y. *Nanotechnology* **2011**, *22*, 175601.
- (6) Manna, L.; Milliron, D. J.; Meisel, A.; Scher, E. C.; Alivisatos, A. P. *Nat. Mater.* **2003**, *2*, 382–385.
- (7) Schulz, K. M.; Abb, S.; Fernandes, R.; Abb, M.; Kanaras, A. G.; Muskens, O. L. *Langmuir* **2012**, *28*, 8874–8880.
- (8) Bishop, K. J. M.; Wilmer, C. E.; Soh, S.; Grzybowski, B. A. *Small* **2009**, *5*, 1600–1630.
- (9) Mann, S. *Nat. Mater.* **2009**, *8*, 781–792.
- (10) Min, Y.; Akbulut, M.; Kristiansen, K.; Golan, Y.; Israelachvili, J. *Nat. Mater.* **2008**, *7*, 527–538.
- (11) Nie, Z.; Petukhova, A.; Kumacheva, E. *Nat. Nanotechnol.* **2010**, *5*, 15–25.
- (12) Deka, S.; Miszta, K.; Dorfs, D.; Genovese, A.; Bertoni, G.; Manna, L. *Nano Lett.* **2010**, *10*, 3770–3776.
- (13) Kim, M. R.; Miszta, K.; Povia, M.; Brescia, R.; Christodoulou, S.; Prato, M.; Marras, S.; Manna, L. *ACS Nano* **2012**, *6*, 11088–11096.
- (14) Miszta, K.; de Graaf, J.; Bertoni, G.; Dorfs, D.; Brescia, R.; Marras, S.; Ceseracciu, L.; Cingolani, R.; van Roij, R.; Dijkstra, M.; Manna, L. *Nat. Mater.* **2011**, *10*, 872–876.
- (15) Qi, W.; de Graaf, J.; Qiao, F.; Marras, S.; Manna, L.; Dijkstra, M. *J. Chem. Phys.* **2013**, *138*, 154504–1–154504–13.
- (16) Qi, W.; Graaf, J. d.; Qiao, F.; Marras, S.; Manna, L.; Dijkstra, M. *Nano Lett.* **2012**, *12*, 5299–5303.
- (17) de Graaf, J.; van Roij, R.; Dijkstra, M. *Phys. Rev. Lett.* **2011**, *107*, 155501.
- (18) Goodman, M. D.; Zhao, L.; DeRocher, K. A.; Wang, J.; Mallapragada, S. K.; Lin, Z. *ACS Nano* **2010**, *4*, 2043–2050.
- (19) Zanella, M.; Bertoni, G.; Franchini, I. R.; Brescia, R.; Baranov, D.; Manna, L. *Chem. Commun.* **2011**, *47*, 203–205.
- (20) Egerton, R. F. *Electron Energy-Loss Spectroscopy in the Electron Microscope*, 3rd. ed.; Springer: New York, 2011.
- (21) Evers, W. H.; Goris, B.; Bals, S.; Casavola, M.; de Graaf, J.; Roij, R. v.; Dijkstra, M.; Vanmaekelbergh, D. *Nano Lett.* **2012**, *13*, 2317–2323.
- (22) Korgel, B. A. *Nat. Mater.* **2010**, *9*, 701–703.
- (23) Modestino, M. A.; Chan, E. R.; Hexemer, A.; Urban, J. J.; Segalman, R. A. *Macromolecules* **2011**, *44*, 7364–7371.
- (24) Xiong, S.; Dunphy, D. R.; Wilkinson, D. C.; Jiang, Z.; Strzalka, J.; Wang, J.; Su, Y.; de Pablo, J. J.; Brinker, C. J. *Nano Lett.* **2013**, *13*, 1041–1046.
- (25) Bigioni, T. P.; Lin, X.-M.; Nguyen, T. T.; Corwin, E. I.; Witten, T. A.; Jaeger, H. M. *Nat. Mater.* **2006**, *5*, 265–270.
- (26) Maki, K. L.; Kumar, S. *Langmuir* **2011**, *27*, 11347–11363.
- (27) Rabani, E.; Reichman, D. R.; Geissler, P. L.; Brus, L. E. *Nature* **2003**, *426*, 271–274.
- (28) Park, J.; Zheng, H.; Lee, W. C.; Geissler, P. L.; Rabani, E.; Alivisatos, A. P. *ACS Nano* **2012**, *6*, 2078–2085.
- (29) Rabideau, B. D.; Pell, L. E.; Bonnecaze, R. T.; Korgel, B. A. *Langmuir* **2006**, *23*, 1270–1274.
- (30) Oliver, S. R. J.; Bowden, N.; Whitesides, G. M. *J. Colloid Interface Sci.* **2000**, *224*, 425–428.
- (31) Bowden, N.; Choi, I. S.; Grzybowski, B. A.; Whitesides, G. M. *J. Am. Chem. Soc.* **1999**, *121*, 5373–5391.
- (32) Bowden, N.; Oliver, S. R. J.; Whitesides, G. M. *J. Phys. Chem. B* **2000**, *104*, 2714–2724.
- (33) de Graaf, J.; Dijkstra, M.; van Roij, R. *J. Chem. Phys.* **2010**, *132*, 164902–1–164902–14.
- (34) de Graaf, J.; Dijkstra, M.; van Roij, R. *Phys. Rev. E* **2009**, *80*, 051405–1–051405–19.
- (35) Hu, S.-W.; Sheng, Y.-J.; Tsao, H.-K. *J. Phys. Chem. C* **2011**, *116*, 1789–1797.
- (36) Rozenberg, B. A.; Tenne, R. *Prog. Polym. Sci.* **2008**, *33*, 40–112.
- (37) Shenhar, R.; Norsten, T. B.; Rotello, V. M. *Adv. Mater.* **2005**, *17*, 657–669.

Supporting information

Self-Assembly of Octapod-shaped Colloidal Nanocrystals into a Hexagonal Ballerina Network Embedded in a Thin Polymer Film

Milena P. Arciniegas[†], Mee. R. Kim^{†§}, Joost De Graaf[‡], Rosaria Brescia[†], Sergio Marras[†], Karol Miszta[†], Marjolein Dijkstra[‡], René van Roij[‡], Liberato Manna^{†}*

[†]Istituto Italiano di Tecnologia (IIT), via Morego 30, IT-16163 Genova, Italy.

[§]Institute for Computational Physics (ICP), University of Stuttgart, Allmandring 3, 70569 Stuttgart, Germany.

[‡]Soft Condensed Matter, Debye Institute for Nanomaterials Science, Utrecht University, Princetonplein 5, 3584 CC Utrecht, The Netherlands.

[‡]Institute for Theoretical Physics, Utrecht University, Princetonplein 5, 3584 CE Utrecht, The Netherlands.

1. Synthesis of octapods:

The synthesis procedure corresponds to those described in previous works by our group.^{1,2} In brief, colloidal CdSe/CdS nanocrystals were synthesized via a one-pot method: CdS pods were grown sequentially on the top of a CdSe seed pre-formed by rapid Cd²⁺-cation exchange of Cu_{2-x}Se nanocrystals in the same reaction flask.

Chemicals: Copper chloride (CuCl, 99.999%), tri-*n*-octylphosphine oxide (TOPO, 99%), tri-*n*-octylphosphine (TOP, 97%), and selenium (Se, 99.99%) were purchased from Strem Chemicals. *n*-Octadecylphosphonic acid (ODPA) and *n*-hexylphosphonic acid (HPA) were purchased from Polycarbon Industries. Propyl phosphonic acid (PPA), cadmium oxide (CdO, 99.99%), cadmium chloride (CdCl₂, 99.99 %), sulfur (S, 99.98%), oleylamine (70%), and 1-octadecene (90%) were purchased from Sigma-Aldrich. Anhydrous methanol and toluene were purchased from Carlo Erba reagents. All chemicals were used as received.

Synthesis of the Cu_{2-x}Se Starting Seeds for Preparing Octapods: All synthesis procedures described here and in the next section were carried out using a standard Schlenk line. The synthesis of Cu_{2-x}Se seeds followed the procedure previously reported.³ 1 mmol of CuCl was mixed with 5 mL of oleylamine and 5 mL of 1-octadecene in a 50 mL three-neck flask. The mixture was heated under vacuum at 80 °C for 1 h and then heated up to 300 °C under N₂ flow. Meanwhile, a selenium precursor solution was prepared by dissolving 0.5 mmol of Se in 4 mL of oleylamine in a 25 mL three-neck flask. The mixture was put under vacuum at 130 °C for 1 h and heated to 230 °C under constant N₂ flow. When the Se was completely dissolved, the solution was cooled down to 180 °C for a fast injection by using a glass syringe equipped with a stainless steel needle into the above copper solution kept at 300 °C. After injection, the reaction was run at

300 °C for another 15 minutes. The flask was then cooled down to room temperature and the resulting black solution was quickly transferred into a N₂-filled vial for the sequent washing steps in a glove box under a N₂ atmosphere. Cu_{2-x}Se nanocrystals were washed by repeated precipitation with methanol and re-dispersion in toluene, and the final seed nanocrystals dissolved in 3 mL of TOP. The concentrations of Cu_{2-x}Se nanocrystals (with average size of 15 nm) in TOP was determined to be around 3·10⁻⁶ M by inductively coupled plasma optical emission spectroscopy on digested solutions (with HCl/HNO₃ 3:1 (v/v)).

Synthesis of CdSe/CdS Octapods: The synthesis procedure was according to those described in previous works by our group.^{1,2} Briefly, 0.060 g of CdO, 0.006 g CdCl₂, 0.305 g ODPA, 0.038 g HPA, 0.025 g PPA and 3.000 g of TOPO were loaded in a 25 mL three-neck flask and heated to 120 °C under vacuum for 1 h. The CdCl₂ amount is the critical factor to obtain very uniform and homogeneous octapod products and the ratio of the three phosphonic acids control the pod length of octapods. The temperature of the mixture was switched to 380 °C under N₂ flow and 2.6 mL of TOP was injected. In the glove box, 100 μL of a 3.0·10⁻⁶ M solution of Cu_{2-x}Se nanocrystals in TOP (corresponding, therefore, to 3.0·10⁻¹⁰ moles of nanocrystals) was mixed with 0.5 g of TOP:S (previously prepared by dissolving 96 mg of S in 1 mL of TOP). The mixture was then injected rapidly into the reaction flask recovered to 380 °C. After the injection, the reaction was run for 10 min and then the reaction solution was cooled to room temperature. The resulting product was purified by washing with toluene and methanol, and finally dispersed in toluene (boiling point of 110.6 °C). Octapod-shaped nanocrystals presented a tip-to-tip length, $2L$, of 97 ± 4 nm and Dp of 12 ± 2 nm ($L/Dp \approx 4.0$), as determined by TEM analysis.

2. Film preparation and structure characterization:

Materials: Polymethyl methacrylate (PMMA) ($M_w = 120.000$ g/mol; $M_w = 350.000$ g/mol; $T_g = 105$ °C), toluene, acetone and isopropanol were purchased from Sigma-Aldrich.

Solutions of PMMA at 0.5, 1, and 5 % vol. in toluene were prepared and mixed with two concentrations of octapods (10^{-7} M and 10^{-8} M) in a 1:4 volume ratio. The mixed solutions were kept under vortex for a few minutes. The samples from both repeatedly-washed octapod solutions, with no polymer added, and octapod-polymer were prepared by drop casting and drying in air on the substrates. Two types of substrates were used: carbon-coated Cu grids for transmission electron microscopy (TEM) and SiO₂ wafers sputter-coated by a 10 nm-thick carbon film. The samples from the surfactant-rich octapod solution were prepared by drop casting of 5 μ l of the solution on a SiO₂ wafer in a toluene-saturated atmosphere to allow slow drying.

Bright field (BF) transmission electron microscopy (TEM) analyses were conducted on a 100 kV JEOL JEM 1011 microscope. Energy-filtered TEM (EFTEM) images were acquired using a JEOL JEM-2200FS ultra-high resolution microscope, equipped with an in-column (Omega) energy filter and operated at 200 kV. The thickness of the PMMA layer embedding the hexagonal-ballerina assemblies was evaluated by computing the ratio between unfiltered BF-TEM and zero-loss filtered (EFTEM) images of octapod-empty regions (log-ratio method).⁴ The inelastic mean free path of the 200 keV electrons through PMMA was calculated by assuming the PMMA molecular formula, $[\text{CH}_2\text{C}(\text{CH}_3)(\text{CO}_2\text{CH}_3)]_n$. A Tecnai G2 F20 TEM, operated at 200 kV acceleration voltages, was used to obtain single-tilt series of high angle annular dark field (HAADF)-scanning TEM (STEM) images of the octapod assemblies. The volume

reconstruction was done for the area in Figure S4 (see also movie SI2.avi) by weighted back-projection followed by 20 SIRT iterations, using the Tomoj plugin of ImageJ.^{5,6} The iso-surface rendering of the volume has been obtained using the UCSF Chimera package.⁷ Scanning electron microscopy (JEOL JSM-7500FA) was conducted on both Carbon-coated film on TEM grids and SiO₂ substrates with a 10 nm sputtered carbon coating. All substrates were cleaned before depositing the drops using 10 minutes of ultrasonic bath in acetone, distilled water and isopropanol. After cleaning they were carefully dried with pressurized air. A plasma reactor (Gambetti Tucano Multipurpose Plasma System) with an oxygen flow was used for the removal of the polymer from the substrates. The plasma exposure time was of 5 min at room temperature with a bias power level of 200 W.

After deposition, the thickness of the films was measured by an AMBiOS XP-2 Technology optical profilometer. Contact angles were determined by the sessile-drop method using OCA20 equipment - Dataphysics Instrument. One polar liquid, ultra pure MilliQ® - Millipore Corporation - was employed; 3 µl droplets were deposited at 1 ml/sec on the surfaces of the samples. The drop image was captured by the video camera and analysed using the SCA20 software. Both SiO₂ and SiO₂ with a sputtered carbon coating substrates were prepared under the same conditions and used as control material.

2. Supplementary figures and discussion:

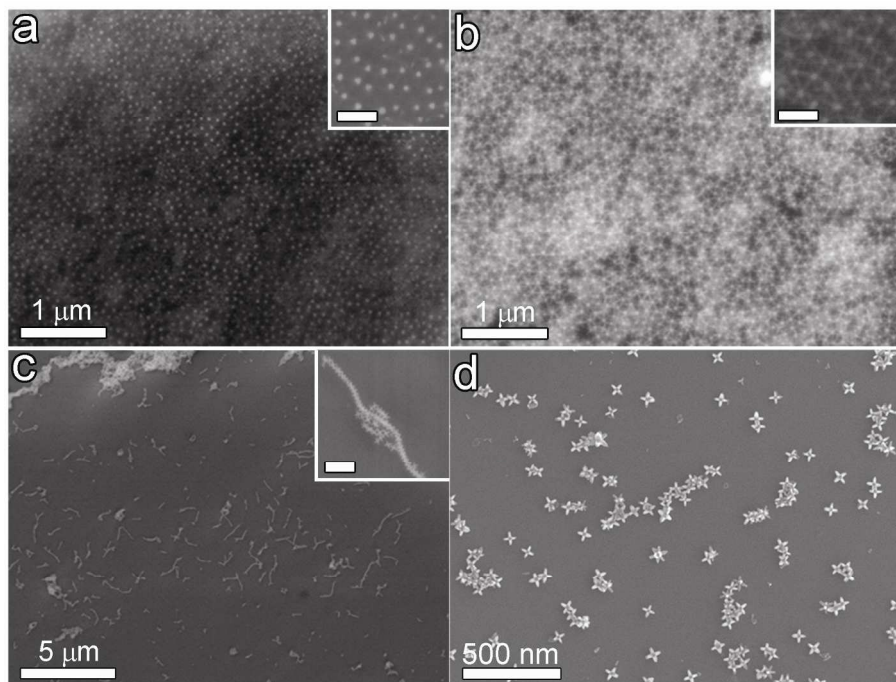


Figure S1. SEM images showing different configurations of octapods by varying the deposition variables. a) Top view of the organic-rich solution of octapods, deposited on a SiO₂ substrate and subsequently allowed to dry slowly, showing the tips of the pods as bright white spots (SEI detector); the inset shows a closer view of the pods protruding from the organic film; scale bar: 100 nm. b) SEM image of the same zone revealing that seven pods of each octapod are embedded in the surfactant layer and confirming that six of these pods form the edges of a hexagonal structure with the surrounding octapods, as is further shown in the inset; scale bar: 100 nm (LBE detector). c) Formation of chain-like structures of octapods after slow evaporation of the purified solution. The inset image shows a closer view of a chain of interlocked octapods; scale bar: 200 nm. d) Octapods with four pods in contact with the substrate (presenting a cross-shape in a top view) after solvent evaporation in open air (fast evaporation) of a solution purified by four washing steps.

Monitoring Octapod-Aggregation in PMMA Solution by Dynamic Light Scattering (DLS)

The formation of aggregates of octapods in solution by the addition of various concentrations of PMMA with two different molecular weights ($M_w = 120.000$ g/mol and $M_w = 350.000$ g/mol) was investigated by Dynamic Light Scattering (DLS) measurements. Figures S2a and S2b show the mean size distribution profiles for the fresh solution of octapods ($200 \mu\text{l}$ of 10^{-7} M) in toluene before and after the addition of five different concentrations of PMMA ($50 \mu\text{l}$) of low and high molecular weight, respectively.

A narrow size distribution was observed from the fresh solution of octapods in toluene without PMMA. Clearly, agglomeration of octapods is produced in the solution by the addition of PMMA for both molecular weights, which is evidenced by the peaks being shifted towards larger sizes, but also by the broader intensity peaks for all the concentrations. This effect becomes stronger by the addition of PMMA with $M_w = 120.000$ g/mol at concentrations higher than 3%, for which the profiles present a bimodal size distribution. Additionally, it is evident that the increase in molecular weight induced a stronger aggregation in the solution from the change in the effective particle size from 92.3 ± 0.4 nm to 380 ± 20 nm (see Fig. S2b). Visual evidence of aggregation was also appreciated by changes in the transparency of the solutions prepared with the higher molecular weight PMMA (see inset in Fig. S2b for 1, 3, and 7% vol. from right to left); while the turbidity of the solutions containing PMMA with $M_w = 120.000$ g/mol was less evident (see inset in Fig. S2a).

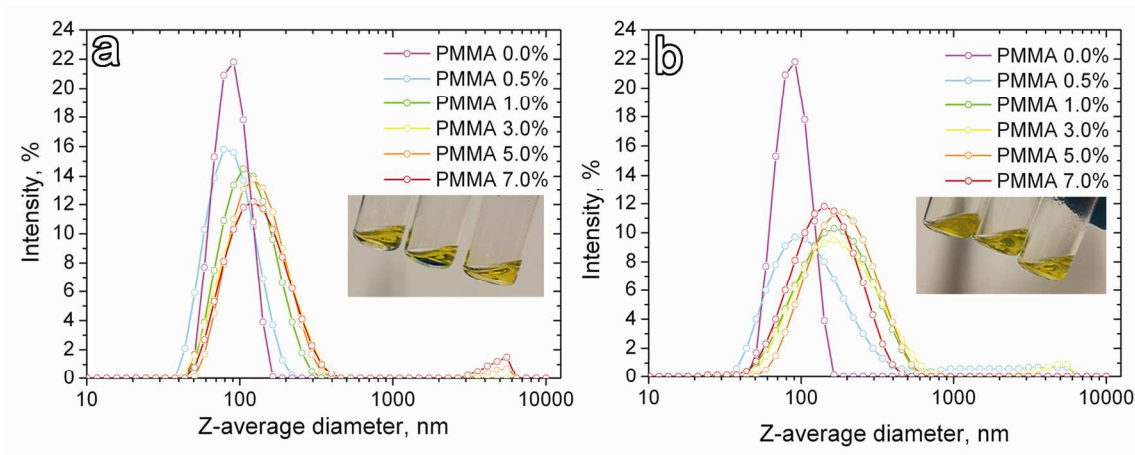


Figure S2. Monitoring octapod-aggregation in PMMA with different molecular weights. Size-distribution profiles obtained by DLS shown the formation of octapod-aggregates by the addition of PMMA with (a) $M_w = 120.000$ g/mol and (b) $M_w = 350.000$ g/mol at different concentrations (% vol.). The inset images show the changes in transparency of the solutions after the addition of the polymer at 1, 3, and, 7 % vol. in toluene from right to left.

Figure S3a shows the TEM images of the PMMA-based nanocomposites prepared at room temperature by solution casting, with a low concentration of octapods (10^{-8} M, $200 \mu\text{l}$) in $50 \mu\text{l}$ of polymer with $M_w = 120.000$ g/mol at 0.5, 1.0, and 5.0 % vol. of polymer ($M_w = 120.000$ g/mol). Only a few octapods were observed to form short-range ordered structures. Figure S3b presents a collection of TEM images for different concentrations of PMMA with $M_w = 350.000$ g/mol, evidencing the formation of aggregates, the size of which decreased with the polymer content in toluene. The increase of the aggregate size for the lowest concentration of PMMA is attributed to the strong effect of polymer dewetting.

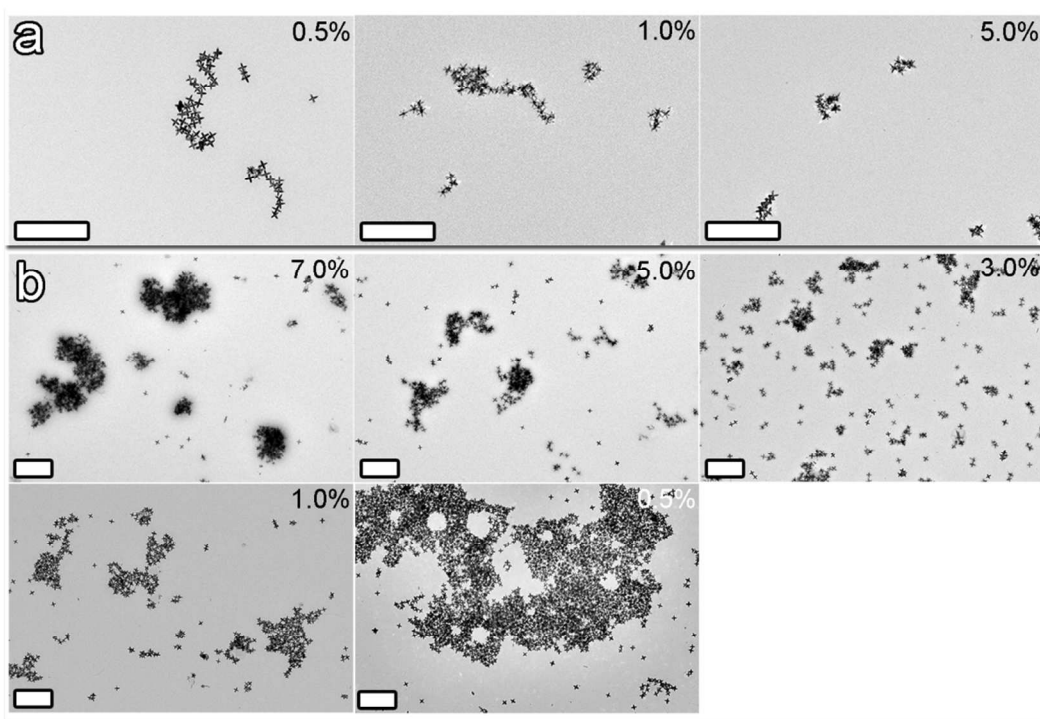


Figure S3. Octapod-aggregation in PMMA with higher molecular weight, $M_w = 350.000$ g/mol. a) TEM images showing the lack of large ordered structures due to the low concentration of octapods, from left to right the PMMA concentration is 0.5, 1.0, and 5.0 % vol. b) TEM images of the PMMA-based nanocomposite revealing the presence of octapod aggregates of increasing size by decreasing the polymer concentration. Octapod concentration: 10^{-7} M, from left to right and top to bottom the PMMA concentration is 7.0, 5.0, 3.0, 1.0, and 0.5 % vol.

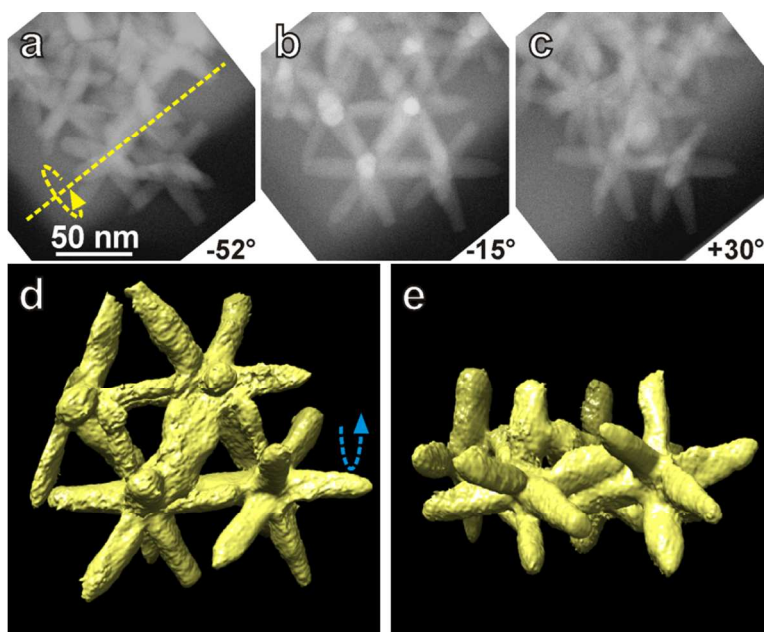


Figure S4. *a-c) HAADF-STEM images extracted from a single tilt series (from -60° to $+70^\circ$) of a small group of octapods showing the ballerina orientation, with parallel pod-to-pod configuration (see supplementary movie SI2.avi for the complete tilt series). The tilt axis direction and rotation direction are indicated in a). d-e) Isosurface view of the volume reconstructed by electron tomography based on the same tilt series, viewed d) from top and e) from side, where the pod-to-pod parallel arrangement among neighboring particles is evident.*

3. Theoretical Investigation of the Wetting of Octapods:

In this section we consider the adsorption of a single octapod at a flat toluene/polymer-air interface using a theoretical model based on surface-tension arguments. We apply a model similar to that of P. Pieranski, who analyzed the strength of adsorption of spherical colloids at liquid-gas and liquid-liquid interfaces.⁸ To describe the experimental system, we consider an octapod as the intersection of four spherocylinders which are oriented in the $(\pm 1, \pm 1, 1)$ directions and which are centered on the origin, similar to the model used in Refs. 9, 10. The tip-to-tip length of these spherocylinders is $2L$, their diameter is D , thus the length of the cylindrical shaft is $2L - D$, and their aspect ratio is given by L/D . In accordance with the experimental results we assumed an aspect ratio of $L/D = 4$.

We also considered a triangular-tessellation-based model similar to that of Ref. 11, again for a pod-to-diameter ratio of 4. The system is modeled as follows. In the spirit of the work by P. Pieranski, we consider the free energy of adsorption of a single octapod to see what its optimal (equilibrium) adsorption configuration is. The configuration of the particle can be described by four parameters: (i) the size of the particle, which is given by the multiplicative factor s ; (ii) the height z of the particle with respect to the interface (as measured along the z -axis) – we locate the interface at $z = 0$ (xy -plane); (iii) rotation by the azimuthal angle ψ (around the z -axis); and (iv) rotation by the polar angle φ (around the y -axis). We assume that the octapod is first scaled by s , then rotated by ψ and subsequently by φ , and finally it is translated by z . Due to the symmetry properties of the octapod we can restrict ourselves to ψ in $[0, \pi/4]$ and φ in $[0, \pi/2]$. Even for this restricted range there are several instances of duplicate orientations, e.g., ψ in $[0, \pi/4]$ and $\varphi = 0$ gives essentially the same configuration as $\psi = 0$ and $\varphi = \pi/2$ for the same value of z . These duplicate configurations are taken into account via congruence in our analysis; see the

Supplementary Information to Ref. 12 for a similar approach. The octapod surface is assumed to have homogeneous surface properties and the two media, air and the toluene/polymer mixture are also assumed to be homogeneous. This is a significant simplification, since in the experiments the surface properties of the different facets are likely different and the media are presumably not homogeneous near the interface. In this system the free energy of adsorption F can be written as

Eq. 1:
$$F(z, \psi, \varphi) = \gamma_{\text{int}}(A - S_{\text{int}}) + \gamma_{\text{oa}}S_{\text{oa}} + \gamma_{\text{om}}S_{\text{om}}$$

where γ_{int} is the liquid-air interfacial tension, A is the total surface area of the interface, S_{int} is the surface area excluded from the interface by the presence of the octapod, γ_{oa} is the surface tension between air and the octapod surface, S_{oa} is the total surface area of the octapod in contact with the air, γ_{om} is the surface tension between toluene/polymer mixture and the octapod surface, and S_{om} is the total surface area of the octapod in contact with the mixture. Note that we have made the dependence of S_{int} , S_{oa} , and S_{om} on (z, ψ, φ) implicit.

In this model, the microscopic degrees of freedom of the solvent molecules were integrated out to yield the surface tensions. We further assumed that the interface is not deformed by the presence of the particle: capillary deformation by gravity, electrostatic effects, or contact-angle requirements. These are strong simplifications, but there are too many unknowns regarding the experimental system to justify a more extended model. In this light, the results obtained in the next section should be seen as an indication of the possible behavior of an octapod at the interface, rather than a full theoretical description of the phenomenology in the experimental system.

To simplify the calculations we can reduce Eq. 1 by subtracting a constant contribution to the free energy of adsorption

$$\text{Eq. 2:} \quad F'(z, \psi, \varphi) = F(z, \psi, \varphi) - [\gamma_{\text{int}}A + \gamma_{\text{oa}}(S_{\text{oa}} + S_{\text{om}}) + \gamma_{\text{om}}(S_{\text{oa}} + S_{\text{om}})];$$

$$\text{Eq. 3:} \quad F'(z, \psi, \varphi) = (\gamma_{\text{oa}} - \gamma_{\text{om}}) S_{\text{oa}} - \gamma_{\text{int}}S_{\text{int}};$$

$$\text{Eq. 4:} \quad F'(z, \psi, \varphi) = \gamma_{\text{int}}[\cos\theta S_{\text{oa}} - S_{\text{int}}],$$

where we set the shifted free energy F' to zero when the colloid is completely immersed in the polymer/toluene mixture. In the last step (Eq. 4) we used Young's equation¹³

$$\text{Eq. 5:} \quad \gamma_{\text{oa}} = \gamma_{\text{int}}\cos\theta + \gamma_{\text{om}},$$

with θ the contact angle corresponding to the octapod - air - polymer/toluene three-phase contact.

Note that θ is determined by material properties, whereas ψ and φ are variables in our theory.

Using the above equations we can now write the dimensionless free energy of adsorption as

$$\text{Eq. 6:} \quad f(z, \psi, \varphi) = F'(z, \psi, \varphi)/(\gamma_{\text{int}}S) = [\cos\theta S_{\text{oa}} - S_{\text{int}}]/S,$$

with $S = S_{\text{oa}} + S_{\text{om}}$ the total surface area. Note that $f(z, \psi, \varphi)$ is independent of the size s of the particle. For a given θ , Eq. 6 gives rise to a three-dimensional (3D) free-energy landscape. This landscape was established by numerically determining the values of the various surface areas on a (z, ψ, φ) grid using the triangular-tessellation technique of Refs. 14, 15 we used 100 equidistantly spaced points in each direction. The thermodynamic equilibrium is assumed in the minimum of the free-energy landscape, i.e., the (z, ψ, φ) combination for which f has the lowest value. The density of grid points allows us to approach the actual minimum on our grid to within a sufficient level of precision to justify further analysis. Note that the presence of metastable

minima in the free energy of adsorption is not taken into consideration by analyzing the lowest free-energy value only.

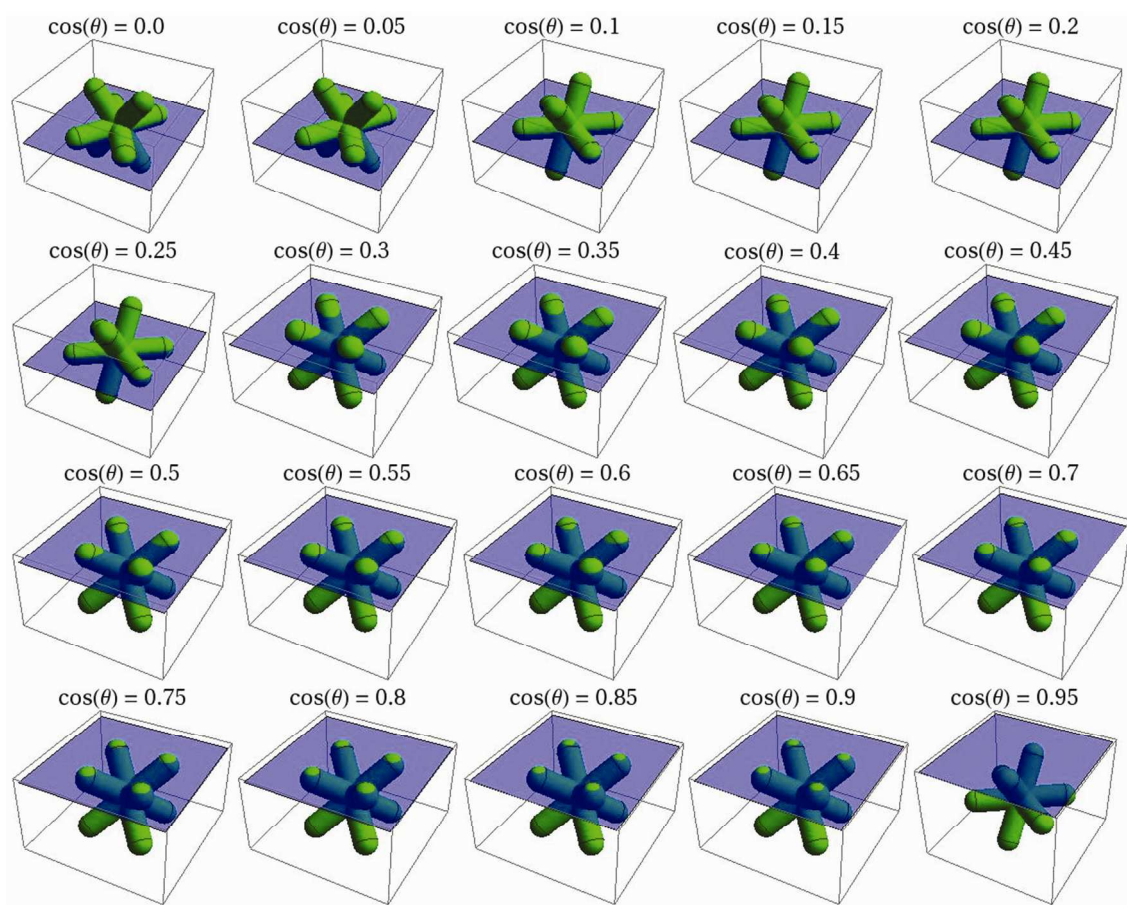


Figure S5. Models for the optimal adsorption configuration of octapods (green spherocylinder model) partially immersed in a polymer monolayer as a function of the octapod wettability given by the cosine of the contact angle $\cos\theta$, which runs from 0.0 to 0.95. The interface is indicated by a transparent blue plane. Negative values of the contact angle result in configurations which are mirrored in the interface. Note that the configuration for the two lowest values of $\cos\theta$ are the same as the configurations for the other low- $\cos\theta$ values, just visualized from a different direction. Also note that the octapod is completely detached from the interface for $\cos\theta = 0.95$.

An advantage of our model is that once the surface areas have been determined establishing $f(z, \psi, \varphi)$ for different values of θ in $[0.0, 0.95]$ is simple. We did not consider negative values of θ since in our model a negative value of θ corresponds to mirroring the system in the interface. Our results, see Fig. S5, showed that the equilibrium orientations of the octapods (the results for the triangular model are not shown here) can be roughly divided into two categories: (I) four-arms lie flat on the interface and two stick out on either side and (II) the octapod rests on the interface with four tips slightly penetrating it (see Fig. S5). These configurations can be grouped under the two archetypical configurations given in the manuscript, since for the contact angles that we considered there are only slight variations with respect to these two. From Fig. S5 it follows that there is a sharp transition from configuration I to configuration II, with no intermediate states.

It is important to note that our results (and the conclusions we based on these) were obtained using a simple model for the adsorption of an octapod to an air-polymer/toluene interface. We leave a full investigation of the experimental phenomenology by theoretical or simulation means as an open problem for future study.

References

1. Kim, M. R.; Miszta, K.; Povia, M.; Brescia, R.; Christodoulou, S.; Prato, M.; Marras, S.; Manna, L. *ACS Nano* **2012**, 6, (12), 11088-11096.
2. Deka, S.; Miszta, K.; Dorfs, D.; Genovese, A.; Bertoni, G.; Manna, L. *Nano Lett.* **2010**, 10, (9), 3770-3776.
3. Korgel, B. A. *Nat. Mater.* **2010**, 9, (9), 701-703.
4. Egerton, R. F., *Electron Energy-Loss Spectroscopy in the Electron Microscope*. 3rd. ed.; Springer: New York, 2011.
5. Abramoff M.D., M. P. J., Ram Sunanda J. *Biophotonics international* **2004**, 11, (7), 36-42.
6. Cédric Messaoudi, T. B., Carlos Oscar Sanchez Sorzano, Sergio Marco. *BMC Bioinformatics* **2007**, 8, 288-296.
7. Pettersen EF, G. T., Huang CC, Couch GS, Greenblatt DM, Meng EC, Ferrin TE. *J. Comput. Chem.* **2004**, 13, 1605-1612.
8. Pieranski, P. *Phys. Rev. Lett.* **1980**, 45, (7), 569-572.
9. Qi, W.; de Graaf, J.; Qiao, F.; Marras, S.; Manna, L.; Dijkstra, M. *J. Chem. Phys.* **2013**, 138, (15), 154504-13.
10. Qi, W.; Graaf, J. d.; Qiao, F.; Marras, S.; Manna, L.; Dijkstra, M. *Nano Lett.* **2012**, 12, (10), 5299-5303.
11. Miszta, K.; de Graaf, J.; Bertoni, G.; Dorfs, D.; Brescia, R.; Marras, S.; Ceseracciu, L.; Cingolani, R.; van Roij, R.; Dijkstra, M.; Manna, L. *Nat. Mater.* **2011**, 10, (11), 872-876.
12. Evers, W. H.; Goris, B.; Bals, S.; Casavola, M.; de Graaf, J.; Roij, R. v.; Dijkstra, M.; Vanmaekelbergh, D. *Nano Lett.* **2012**, 13, (6), 2317-2323.
13. Young, T. *Phil. Trans. R. Soc. London* **1805**, 95, 65-87.
14. de Graaf, J.; Dijkstra, M.; van Roij, R. *J. Chem. Phys.* **2010**, 132, (16), 164902.
15. de Graaf, J.; Dijkstra, M.; van Roij, R. *Phys. Rev. E.* **2009**, 80, (5 Pt 1), 051405-19.